J Biol Inorg Chem (2011) 16:1255–1268
DOI 10.1007/s00775-011-0813-8

ORIGINAL PAPER

The mechanism of formate oxidation by metal-dependent formate dehydrogenases

Cristiano S. Mota · Maria G. Rivas · Carlos D. Brondino · Isabel Moura · José J. G. Moura · Pablo J. González · Nuno M. F. S. A. Cerqueira

Received: 7 February 2011 / Accepted: 20 June 2011 / Published online: 20 July 2011

Abstract Metal-dependent formate dehydrogenases (Fdh) from prokaryotic organisms are members of the dimethyl sulfoxide reductase family of mononuclear molybdenum-containing and tungsten-containing enzymes. Fdhs catalyze the oxidation of the formate anion to carbon dioxide in a redox reaction that involves the transfer of two electrons from the substrate to the active site. The active site in the oxidized state comprises a hexacoordinated molybdenum or tungsten ion in a distorted trigonal prismatic geometry. Using this structural model, we calculated the catalytic mechanism of Fdh through density functional theory tools. The simulated mechanism was correlated with the experimental kinetic properties of three different Fdhs isolated from three different *Desulfovibrio* species. Our studies indicate that the C–H bond break is an event involved in the rate-limiting step of the catalytic cycle. The role in catalysis of conserved amino acid residues involved in metal coordination and near the metal active site is discussed on the basis of experimental and theoretical results.

Keywords Formate dehydrogenase · Reaction mechanism · Molybdenum · Tungsten · Density functional theory

Abbreviations

DFT	Density functional theory
ES	Enzyme–substrate
Fdh	Formate dehydrogenase
PDB	Protein Data Bank
SeCys	Selenocysteine
S_i	Inorganic sulfur atom
Tris–HCl	Tris(hydroxymethyl)aminomethane hydrochloride

Introduction

Formate dehydrogenases (Fdhs) catalyze the oxidation of formate to carbon dioxide according to the reaction [1]

$$HCOO^- \rightarrow CO_2 + H^+ + 2e^- \quad E^\circ = -461 \text{ mV (pH 8.00)}.$$

In anaerobic prokaryotes, the oxidation of formate is used as the main electron source for a variety of pathways that use as the final electron acceptor molecules other than

Electronic supplementary material The online version of this article (doi:10.1007/s00775-011-0813-8) contains supplementary material, which is available to authorized users.

C. S. Mota · M. G. Rivas · I. Moura · J. J. G. Moura (✉) · P. J. González (✉)
REQUIMTE, Departamento de Química,
Centro de Química Fina e Biotecnologia,
Faculdade de Ciências e Tecnologia,
Universidade Nova de Lisboa,
2829-516 Caparica, Portugal
e-mail: jose.moura@dq.fct.unl.pt

P. J. González
e-mail: pablo.gonzalez@dq.fct.unl.pt

C. D. Brondino
Departamento de Física,
Facultad de Bioquímica y Ciencias Biológicas,
Universidad Nacional del Litoral,
S3000ZAA, Santa Fe, Argentina

N. M. F. S. A. Cerqueira (✉)
REQUIMTE, Departamento de Química,
Faculdade de Ciências, Universidade do Porto,
Rua do Campo Alegre s/n, 4169-007 Porto, Portugal
e-mail: nscerque@fc.up.pt

dioxygen. Formate oxidation might also be part of a mechanism to form a proton gradient, once small uncharged molecules such as formic acid can cross the cytoplasmic membrane to the periplasmic space and release two protons after oxidation [2, 3].

Prokaryote Fdhs are metalloenzymes with different subunit composition containing either molybdenum or tungsten at the active site. The crystal structures of three of these enzymes have been reported. The molybdenum-containing enzymes are Fdh-H and the membrane-bound Fdh-N from *Escherichia coli* K12 [4–10]. The tungsten-containing enzyme is the periplasmic Fdh from the sulfate-reducing bacterium *Desulfovibrio gigas* [9–12]. The large subunit of these three enzymes (80–110 kDa) contains the active site and one electron transfer center of the type [4Fe–4S]. In addition, they share high primary sequence identity and have a very similar polypeptide fold [9]. In the oxidized state, the active site contains either a Mo(VI) or a W(VI) ion hexacoordinated in a distorted trigonal prismatic geometry to four sulfur atoms from two pyranopterin molecules, one selenium atom from a selenocysteine (SeCys), and one inorganic sulfur atom, hereafter called S_i (Fig. 1a). Two conserved arginine and histidine residues close to the metal ion, although not involved in metal coordination, were suggested to have key roles in catalysis [4, 13]. In contrast, the crystallographic structure of the reduced molybdenum-containing *E. coli* Fdh-H (i.e., enzyme incubated with the substrate under anaerobic conditions) shows a pentacoordinated molybdenum ion in a distorted square-pyramidal geometry, in which the four sulfur atoms from the two pyranopterin molecules occupy the vertices of the equatorial plane and the S_i ligand is in the apical position (Fig. 1b) [13]. The S_i ligand was firstly proposed to be an oxygenic species [4] but was later identified as a sulfur atom from structural studies of *D. gigas* tungsten-containing Fdh and the reevaluation of the crystallographic data of *E. coli* Fdh-H in the reduced state [12, 13]. The latter also showed that the SeCys ligand is not coordinated to the molybdenum ion in the reduced form of the enzyme (Fig. 1b). Although the structure of a reduced Fdh was only determined for *E. coli* Fdh-H, spectroscopic studies performed on the Fdh from *Desulfovibrio desulfuricans* ATCC 27774 suggest that all molybdenum-dependent Fdhs have similar characteristics in their oxidized and reduced states [14, 15].

Kinetic and spectroscopic data of *E. coli* Fdh-H showed that the oxidation of formate implies the cleavage of the C–H bond to give a CO_2 molecule, and that the α proton of the substrate is transferred to an acceptor group located near the molybdenum ion [4, 5]. On this basis and from structural data, two rather different mechanisms have been proposed by Boyington et al. [4] and Raaijmakers and Romao [13]. Both proposals involve the binding of the formate molecule to the molybdenum ion and the SeCys residue as the proton acceptor group, but differ essentially in how the molybdenum–formate interaction occurs. The formate–active site interaction in the proposal by Raaijmakers and Romao, which is based on the structures depicted in Fig. 1, occurs after breaking of the Se–Mo bond, with the S_i ligand being coordinated to molybdenum along the catalytic cycle. In contrast, the leaving group in the mechanism of Boyington et al. is an OH ligand, now

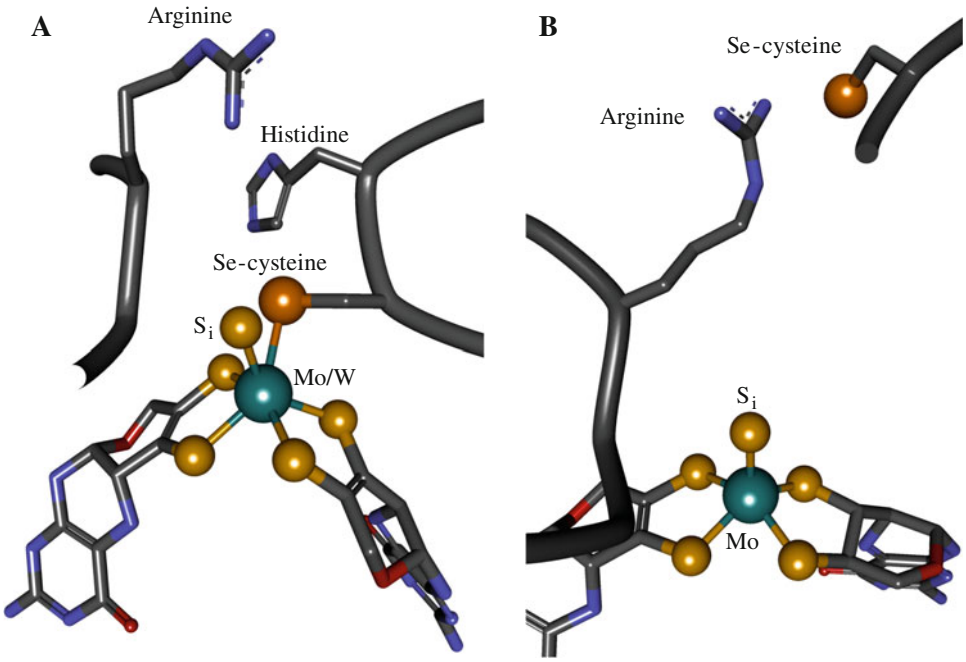

Fig. 1 **a** Coordination around the metal ion of oxidized molybdenum/tungsten-containing formate dehydrogenase (Fdhs) [Protein Data Bank (PDB) ID 1H0H or 1FDO]. **b** Reduced form of *Escherichia coli* Fdh-H (PDB ID 2IV2). Conserved residues of selenocysteine (*Se-cysteine*), histidine, and arginine are also included. *S_i* inorganic sulfur atom

assigned to the S_i ligand (Fig. 1a), and the Se ligand is coordinated to molybdenum along the entire catalytic cycle [4]. Both mechanisms were assessed by Leopoldini et al. [16] using theoretical and computational means. These authors concluded that the SeCys residue is the proton-accepting group and that the mechanism of Raaijmakers and Romao is kinetically and thermodynamically more favorable than that of Boyington et al. (activation energies of 19 and 36 kcal/mol, respectively) [16]. However, Leopoldini et al. only studied the proton abstraction reaction, and avoided in their analysis essential aspects for the catalysis such as the role of the conserved histidine and arginine residues, as well as the processes of substrate binding and product release.

In the work reported here, the catalytic mechanism of Fdh was simulated using density functional theory (DFT) tools and correlated with experimental kinetic data obtained in three Fdhs isolated from *Desulfovibrio* species. This procedure allowed us to address how the enzyme–substrate (ES) interaction occurs, the role of the amino acid residues close to the active site, the conformational changes experienced by the metal site, and the relevance of the metal ions molybdenum and tungsten in the catalysis.

Materials and methods

Bacterial strain, culture media, and growth conditions

D. desulfuricans ATCC 27774, *D. gigas* NCIB 9332, and *Desulfovibrio alaskensis* cells were, respectively, grown in lactate–nitrate [17], lactate–sulfate [18], and in a modified medium C from Postgate [19]. Cells were grown under anaerobic conditions at 37 °C and collected by centrifugation at the end of the exponential phase.

Enzyme purification

Molybdenum-containing Fdh from *D. desulfuricans* ATCC 27774 was purified as described by Rivas et al. [15]. Tungsten-containing Fdh from *D. alaskensis* was purified as described by Mota et al. [19]. Tungsten-containing Fdh from *D. gigas* was purified with a method different from that reported before [20]. The soluble extract was loaded onto a column with DE-52 resin (Whatman) equilibrated with 10 mM tris(hydroxymethyl)aminomethane hydrochloride (Tris–HCl). Elution was performed using a linear gradient from 10 to 500 mM Tris–HCl in 5 column volumes. The fractions containing Fdh were dialyzed and loaded onto a Source 15Q column (GE Healthcare) equilibrated with 5 mM Tris–HCl and were eluted using a linear gradient until 300 mM Tris–HCl in 10 column volumes. The fractions containing Fdh activity were pooled and loaded onto a hydroxyapatite column equilibrated with 1 mM potassium phosphate buffer and were eluted using a linear gradient until 300 mM potassium phosphate buffer in 10 column volumes. Finally, the fraction containing Fdh was concentrated by ultrafiltration in a Centricon system (Amicon) and loaded onto a Superdex 200 column equilibrated with 300 mM Tris–HCl. All the purification steps were performed at 4 °C and pH 7.60.

Enzyme kinetic assays

Steady-state kinetic studies of all Fdhs were performed under an argon atmosphere at 37 °C by monitoring the benzyl viologen reduction at 555 nm ($\varepsilon = 12\ mM^{-1}cm^{-1}$) as described by Rivas et al. [15]. For the study of the isotopic effect, sodium formate was replaced by sodium formate labeled with deuterium at the α-position (99% ^2H, Cambridge Isotopes).

Theoretical calculations

The model chosen to study the catalytic mechanism of Fdh includes a molybdenum (or tungsten) bis(dimethyl dithiolene) complex, in which the ligands represent a portion of the pyranopterinic cofactor. The coordination sphere of the molybdenum (or tungsten) center was completed with a sulfur atom, and a $SeCH_3$ group that was chosen to mimic the $SeCys^{140}$ residue. The model was subsequently completed with the conserved His^{141}, Arg^{333}, and Val^{139} residues (amino acid numbering corresponding to *E. coli* Fdh-H) [4, 6, 7, 12, 13]. Conventional protonation states for all amino acids at pH 7 were adopted and the carboxylate and the amino groups of the terminal amino acids of each chain of the model were protonated. This means that the C-terminus of each amino acid of the model was replaced by an aldehyde group and the N-terminus was replaced by an amine group. For the calculations, the position of the atoms marked with the letter *F* in Fig. 2 was frozen in order to keep the optimized structures close to the X-ray structure.

Several methods are available to study chemical reactions, including static quantum approaches or even advanced sampling techniques, e.g., umbrella sampling [21], metadynamics [22–24], and parallel tempering [25]. In this work, the reaction mechanism was explored using the static quantum approach [26].

The starting coordinates were taken from the 2.80-Å resolution X-ray structure of the oxidized form of *E. coli* Fdh-H (PDB ID 1FDO), where the oxygen ligand to the molybdenum ion was replaced by a sulfur atom. All geometry optimizations were performed with Gaussian 03 [27], applying DFT methods and the 6–31G(d) basis set. Becke's [28] three-parameter exchange functional was used together with the functional of Lee et al. [29]

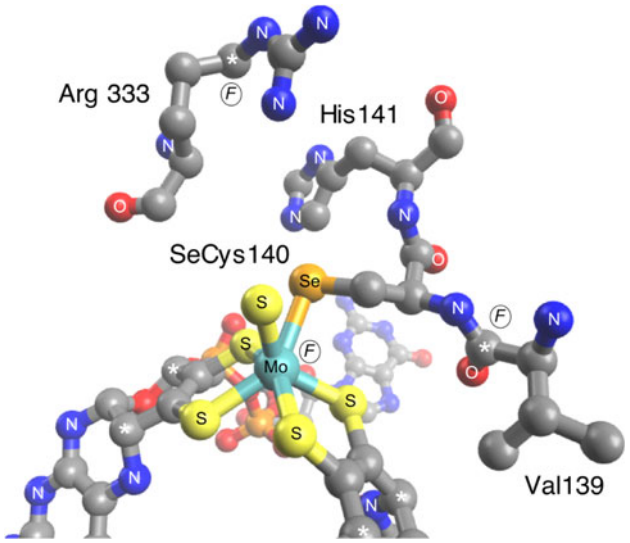

Fig. 2 Model used to study the catalytic mechanism of Fdh (frozen atoms are marked with an *F* and the truncation of the residues is marked with a *white asterisk*, PDB ID 1FDO)

(B3LYP) as implemented in Gaussian [30, 31]. In all geometry optimizations, we first searched for the transition state starting from a structure similar to the reactants model. This was generally obtained with a scan where the reaction coordinate in which we were interested was shortened or stretched. Once the transition state had been located, the reactants and the products associated with it were determined through internal reaction coordinate calculations. In all cases, the geometry optimizations and the stationary points were obtained with standard Gaussian convergence criteria. The transition state structures were all verified by vibrational frequency calculations, having exactly one imaginary frequency with the correct transition vector even when frozen atoms were used, which shows that the frozen atoms are almost free from steric strain.

The final electronic energies were calculated using the all-electron 6–311++G(3df,2pd) basis set. Zero-point corrections, thermal effects, and entropic effects ($T = 310.15$ K, $P = 1$ bar) were added to all calculated energies with the 6–31G(d) basis set [26]. To estimate solvation effects of the rest of the enzyme, single-point calculations on the optimized geometries were performed with the conductor-like polarizable continuum model, as implemented in Gaussian 03 [27], with the B3LYP/6–311++G (3df,2pd) level. This feature is of particular importance in the study of enzymatic catalysis because a continuum model is normally used as an approximation of the effect of the global enzyme environment in a reaction. A dielectric constant of $\varepsilon = 4$ was chosen to describe the protein environment of the active site in accordance with previous suggestions [16, 32–34]. The atomic spin-density distributions were calculated at the B3LYP level by employing a Mulliken population analysis using the 6–31G(d) basis set [35].

Results

Steady-state kinetic studies

The kinetic parameters of the three Fdhs isolated from sulfate-reducing bacteria are given in Table 1 together with those of Fdh-H isolated from *E. coli* K12. The K_m and k_{cat} values of the molybdenum- and tungsten-containing Fdh enzymes isolated from *Desulfovibrio* species are of the same order of magnitude, suggesting that the enzyme as a whole rather than the type of metal in the active site (molybdenum or tungsten) is responsible for the turnover rate and specificity. This is in line with DFT calculations that confirmed that changing molybdenum for tungsten in the active site model does not significantly modify the activation (E_a) and the reaction (E_r) energies of the rate-limiting step of the catalytic mechanism (not shown), and hence it will not be discussed further.

As shown in Table 1, Fdhs from sulfate-reducing bacteria catalyze deuterioformate oxidation with no significant variations of the K_m values with respect to the reactions with formate with natural isotope composition, but the k_{cat} values dropped approximately 2–3 times. This indicates that the formate α-proton transfer to the accepting group is involved in the rate-limiting step of the catalytic mechanism, a fact which was assessed with DFT calculations as

Table 1 Kinetic parameters obtained through steady-state enzyme kinetic studies of molybdenum-containing formate dehydrogenases (*Mo-Fdh*) and tungsten-containing formate dehydrogenases (*W-Fdh*)

	k_{cat} (s^{-1})		K_m (μM)		k_{cat}/K_m		Reference
	$HCOO^-$	$DCOO^-$	$HCOO^-$	$DCOO^-$	$HCOO^-$	$DCOO^-$	
Desulfovibrio desulfuricans Mo-Fdh	347	104	64	81	5.4	1.3	This work
Desulfovibrio gigas W-Fdh	174	96	51	66	3.4	1.5	This work
Desulfovibrio alaskensis W-Fdh	241	191	10	9	24.1	21.2	This work
Escherichia coli K12 Mo-Fdh-H	1,367	1,133	13,300	49,500	0.1	0.02	[36]

Enzyme kinetic plots are reported in Fig. S2.

described later. A different behavior was observed for *E. coli* Fdh-H (see kinetic parameters in Table 1), which is attributed to the presence of azide (which is necessary to preserve enzyme activity during purification) in the enzyme preparations [36]. This was corroborated by adding sodium azide to *D. desulfuricans* Fdh preparations in concentrations similar to that used in the *E. coli* Fdh-H purification, which resulted in lower k_{cat} values that are not affected by the substrate employed ($^1HCOO^-$ or $^2HCOO^-$, not shown). This is in line with EPR results of azide-incubated *D. desulfuricans* Fdh that showed molybdenum signals identical to those of *E. coli* Fdh-H [15].

DFT calculations

Structure and oxidation state of the active site

In metal coordination environments rich in sulfur ligands such as the one studied here for the molybdenum ion, it is difficult to determine the formal oxidation state of the atoms composing the model. For this reason it was assumed that each dimethyl dithiolate ligand ($[H_6C_4S_2]^{2-}$) has a net charge of −2, $SeCH_3$ has a charge of −1, and the S_i has a charge of −2.

Since molybdenum (or tungsten) can be found in these enzymes in three different oxidation states (Mo^{4+}, Mo^{5+}, or Mo^{6+}), our first task was to determine the formal oxidation state of the metal ion in the X-ray structures of the oxidized and reduced forms of Fdh. For this purpose, the hexacoordinated model of the active site described in "Theoretical calculations" was optimized assuming formal oxidation states of Mo^{4+} (charge −3, multiplicity 1), Mo^{5+} (charge −2, multiplicity 2), and Mo^{6+} (charge −1, multiplicity 1). The resulting structures obtained after optimization are depicted in Fig. 3.

The calculations revealed that the structures optimized assuming Mo^{4+} and Mo^{5+} ions are very similar (Fig. 3). In both cases, the selenium atom is found approximately 6.1 Å from the S_i, which remains bound to the molybdenum ion with a bond length of approximately 2.2 Å. These observations are in line with the X-ray structure of the formate-reduced *E. coli* Fdh-H (PDB ID 2IV2), in which the SeCys residue is stabilized with a neighboring arginine by hydrogen bonds 11 Å from the molybdenum ion [13]. Only when the formal oxidation state Mo^{6+} is assumed the selenium atom remains bound to the molybdenum ion and to the S_i ligand at approximately 2.9 and 2.3 Å, respectively (Fig. 3).

The different conformational arrangements of the SeCys residue observed in the three models can be explained taking into account the charge distribution. The total negative charge of the system is higher in the Mo^{4+} and Mo^{5+} models. A Mulliken population analysis reveals that the charge is mainly located at the selenium atom (−0.71 a.u. for Mo^{4+} and −0.67 a.u for Mo^{5+}), the S_i (−0.68 a.u. for Mo^{4+} and −0.47 a.u. for Mo^{5+}), and at the dimethyl dithiolenes (−0.9 a.u. for Mo^{4+} and −0.4 a.u. for Mo^{5+}). This charge distribution creates a repulsive environment between selenium and S_i ligands that produces the dissociation of the SeCys residue. In fact, DFT calculations performed to evaluate the formation of the ES complex with the Mo^{4+} and Mo^{5+} models yielded activation energies of approximately 50 kcal/mol, which rules out the catalysis starting with the enzyme in the Mo^{4+} and Mo^{5+} forms.

The Mulliken population analysis in the Mo^{6+} model reveals that the negative charge is distributed on the dimethyl dithiolene ligands (−0.4 a.u.) and the molybdenum ion (−0.4 a.u.). In contrast to the other two models, the S_i ligand is neutral (0.05 a.u), which, as will be seen

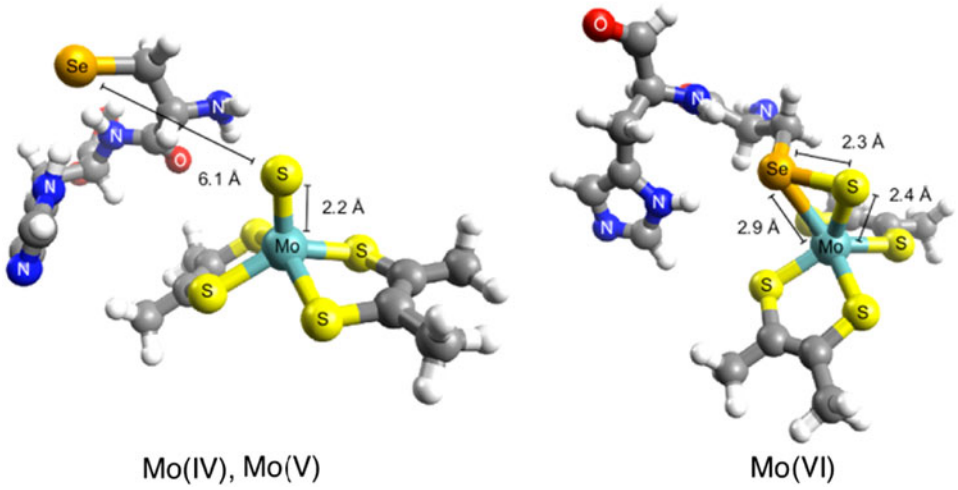

Fig. 3 Optimized structure of the active site models of Fdh assuming Mo^{4+}, Mo^{5+}, and Mo^{6+} formal oxidation states

later, favors the interaction of the substrate with the active site.

The charge distribution in the three models determines the type of interaction that the S_i ligand has with the molybdenum atom. The shorter bond length (2.2 Å) observed in the Mo^{4+} and Mo^{5+} models suggests that the S_i ligand might be double-bonded to the molybdenum, whereas in the Mo^{6+} model the distance (2.4 Å) suggests that the S_i ligand is single-bonded to the molybdenum ion and to the SeCys residue (Fig. 3).

Formation of the ES complex: the selenium–sulfur shift

Taking into account the results described already, one can assumed that the formal oxidation state Mo^{6+} represents the oxidized X-ray structure (Figs. 1a, 3). However, in the course of this study it was found that formate binds the active site only if the Se–S_i bond is previously broken. This is achieved by increasing the Se–S_i distance from 2.25 to 3.56 Å, which requires 15.5 kcal/mol and is endothermic by 7.5 kcal/mol (Scheme 1). The transition state for this reaction is characterized by one imaginary frequency at 75.72i cm^{-1}. After this rearrangement, both atoms remain bound to the molybdenum ion but with different bond lengths (Se–Mo bond length from 2.39 to 2.59 Å, S_i–Mo bond length from 2.91 to 2.16 Å). At this stage, the partial interaction of the formate anion produces a redistribution of the charge in the metal complex. This is observed because the charges of the S_i and molybdenum–bis(dimethyl dithiolene) change from −0.26 to −0.60 a.u. and from −0.62 to −0.08 a.u., respectively.

Experimental evidence from EPR spectroscopy and X-ray crystallography suggests that the formate molecule reacts with the molybdenum ion [4, 5, 13, 15]. The Mo^{6+} model obtained in this study has, however, revealed that the Se–S_i–Mo complex does not have an available binding site for the formate to bind the molybdenum, indicating that the formation of the ES complex is not a straightforward process. Our studies showed that when the oxygen of the formate molecule moves toward the S_i ligand (−0.53 a.u.), it pushes the S_i ligand to the position originally occupied by the selenium atom, forcing the dissociation of the SeCys residue from the molybdenum ion (Mo–Se distance from 2.72 to 4.11 Å). In this process, Arg^{333} has a key role driving the formate molecule toward the S_i ligand through two strong hydrogen bonds (1.74 Å). Because of the repulsive environment generated by the approximation of the formate anion toward the negatively charged metallic complex, this reaction requires 20.0 kcal/mol (Scheme 2). However, this high energetic barrier is compensated as the reaction is exothermic (−5.7 kcal/mol) and ends with the formate molecule bound to the molybdenum ion by a single bond (2.14 Å). The S_i also remains single-bonded to the molybdenum at 2.50 Å and loses its negative charge (−0.06 a.u.). At this stage, the SeCys residue dissociates from the molybdenum, but remains covalently bound to the S_i (2.26 Å).

The transition state of this reaction (characterized by one imaginary frequency of 119.62i cm^{-1}) clearly

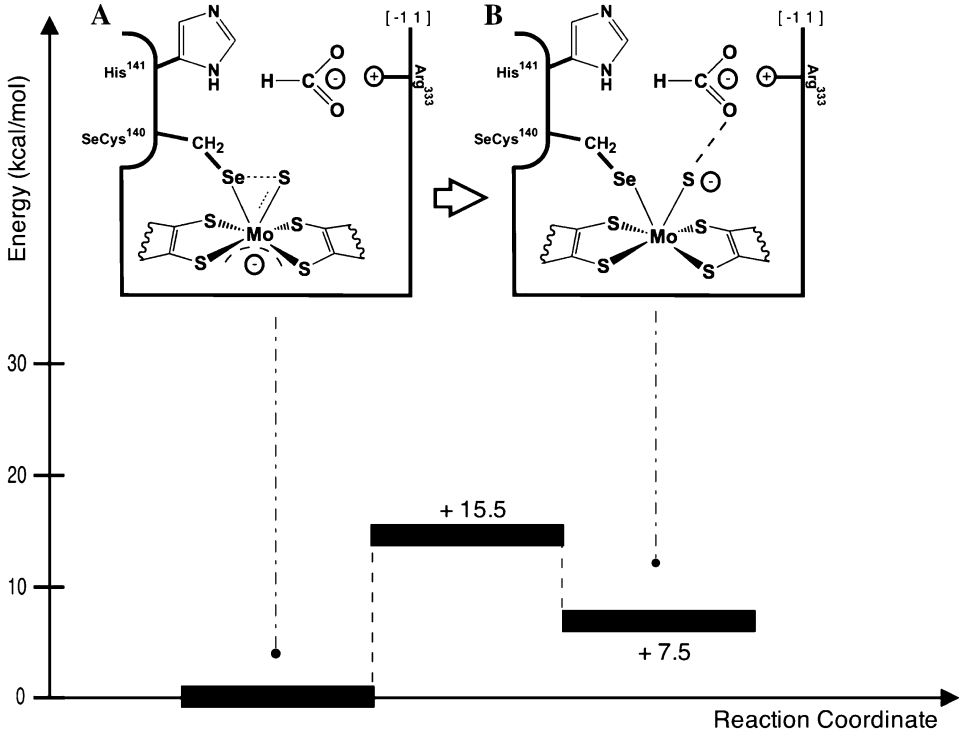

Scheme 1 Enzyme–substrate (ES) interaction (the total charge and multiplicity of the system are in *brackets*)

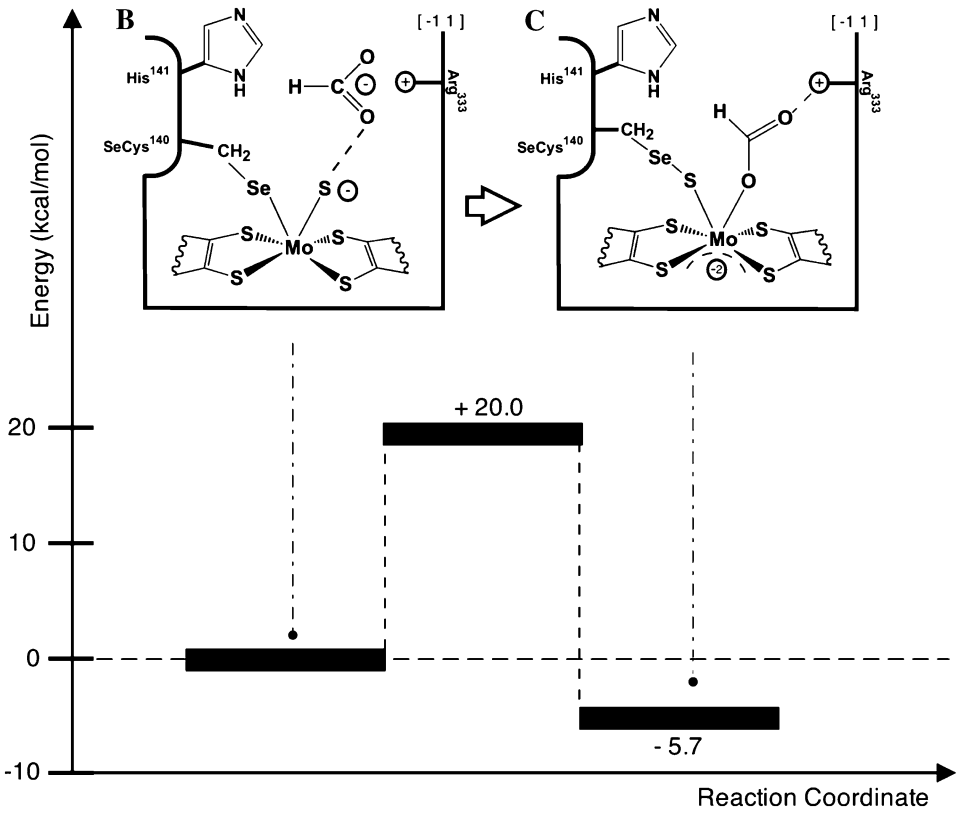

Scheme 2 Proposed selenium–sulfur shift during the formation of the ES complex (the total charge and multiplicity of the system are in *brackets*)

demonstrates the feasibility of three events in one step: (1) dissociation of the SeCys residue from the molybdenum ion (selenium shift), (2) conformational rearrangement of the S_i (sulfur shift) and, (3) coordination of the formate molecule to the molybdenum ion.

This reaction is only possible owing to the presence of the molybdenum–dithiolene complex and the conserved Arg^{333} that act to buffer the negative charge of the formate anion (the charge of the molybdenum–dithiolene complex changes from −0.13 to −0.72 a.u.). This type of behavior was also proposed for the catalytic mechanism of the periplasmic nitrate reductase, where the nitrate anion binds a similar negatively charged active site [37]. These results suggest that one of the roles of the pyranopterinic cofactors in these enzymes might be, in addition to providing an electron transfer pathway [9, 10], to cushion the electrostatic repulsion produced by the negative charge of formate, lowering the activation energy barrier for the formation of the ES complex.

Selenide anion formation and formate oxidation

The oxidation of the formate molecule to carbon dioxide involves the transfer of either a proton or a hydride from formate to a neighboring atom. Two atoms could accomplish this function: the selenium atom from the SeCys residue or the S_i. Our results revealed that this step is only possible with the participation of the SeCys residue. Moreover, it was observed that His^{141} is also very important for this reaction, since the exclusion of His^{141} from the model yielded an activation energy of approximately 45 kcal/mol.

Computational results including His^{141} indicated that formate oxidation occurs via the formation of a selenide anion, which implies that the Se–S_i bond must be broken in a reaction that is not energetically favorable owing to the instability of the product. In this sense, the SeCys residue dissociation reaction requires $E_a = 18.4$ kcal/mol and is endothermic by 16.7 kcal/mol (Scheme 3). In the reactants, the selenium atom is covalently bound to the S_i (2.65 Å), which is also bound to the molybdenum ion (2.24 Å). As the Se–S_i bond length is stretched, the selenium atom forms a hydrogen bond with one NH group of the imidazole ring of the conserved His^{141}, which lowers E_a. In the optimized structure of the transition state (40i cm^{-1}), the selenium atom is almost dissociated from the S_i (3.20 Å), whereas His^{141} undergoes a conformational rearrangement in which the NH group is aligned with the selenium atom to form a hydrogen bond. In the product of the reaction, the Se–S_i bond is broken (4.44 Å), and the selenide anion (with a charge of −0.83 a.u.) is formed. In this stage of the reaction the NH group from the histidine imidazole and the selenium atom are 2.56 Å apart, indicating the important role of the conserved His^{141} in stabilizing the selenide anion

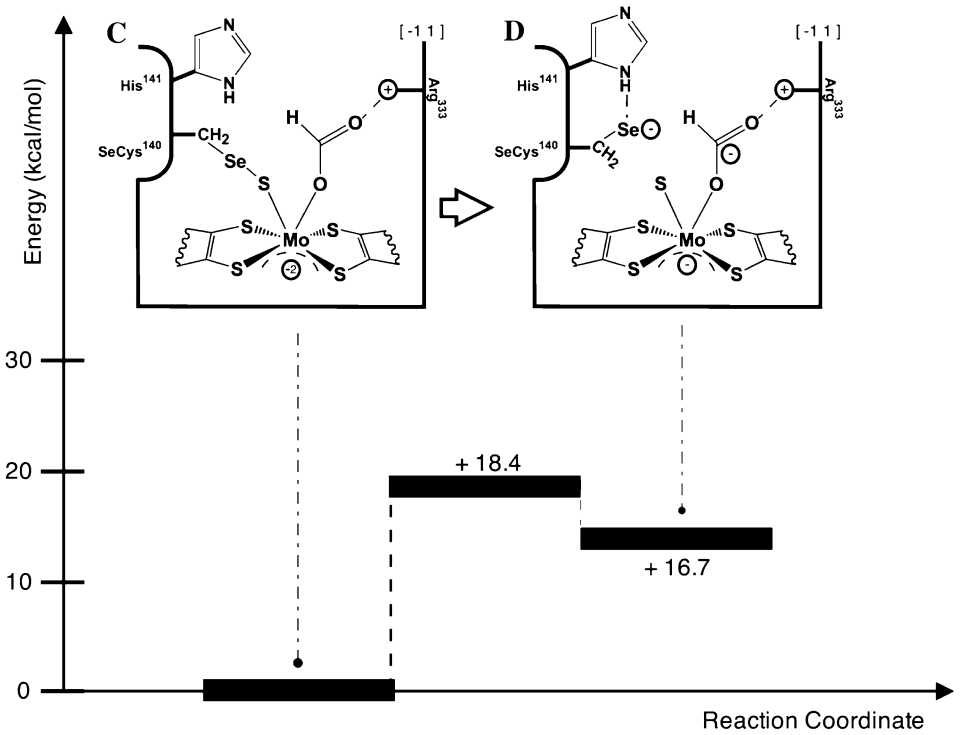

Scheme 3 Selenide anion formation (the total charge and multiplicity of the system are in *brackets*)

that will perform the proton abstraction. We also tested the hypothesis of the proton transfer between the formate molecule and the selenium atom in one concerted step, i.e., with the selenium atom binding the S_i ligand. However, E_a values of approximately 45 kcal/mol were obtained.

The next step, which comprises the formate oxidation per se, starts with the selenide anion positioned 3.84 Å from the formate hydrogen (Scheme 4). During the search for the transition state for this reaction, it became clear that when the Se–$H_{formate}$ distance is shortened, the S_i–$C_{formate}$ distance also decreases. This is evident in the transition state of this reaction (589.48i cm^{-1}), in which the selenium atom is found 1.89 Å from the formate hydrogen and the S_i is found 2.15 Å from the formate carbon (3.30 Å in the reactants).

The optimized structure of the transition state also revealed that a proton with charge of +0.81 a.u. is transferred to the SeCys residue, which is in agreement with the results reported by Leopoldini et al. [16]. It is possible that the S_i has some role in the proton transfer between the formate and SeCys residue since the Si–$H_{formate}$ distance found in the transition state of the reaction in Scheme 4 is as low as 2.35 Å.

In the product of the reaction depicted in Scheme 4, the SeCys residue is protonated and moves away from the active site (Mo–Se distance 7.66 Å). Consequently, the hydrogen bond between the selenium atom and the His^{141} residue is broken and a new hydrogen bond between the S_i and His^{141} is formed (2.53 Å). The carbon from the –CO_2 group is now bound to the S_i at a distance of 1.78 Å, and one of the oxygens from the –CO_2 remains bound to the molybdenum ion (Fig. 4).

The proton transfer reaction requires 21.2 kcal/mol and is exothermic by −27.7 kcal/mol (Scheme 4), indicating that despite the relatively high activation energy barrier of the two steps, this reaction is feasible. It is important to mention that a high E_a value was expected for this step owing to the primary isotopic effect observed with deuterium-labeled sodium formate in the enzyme kinetic studies mentioned before (Table 1).

Carbon dioxide release

The next step of the catalytic cycle involves the release of carbon dioxide and the two-electron oxidation of the active site. This can be accomplished in two different ways: (1) the carbon dioxide is released before the oxidation of the active site or (2) the active site is oxidized to promote the product release.

In the first case, the dissociation of the CO_2 requires the two steps depicted in Scheme 5. Firstly, the Mo–O bond is broken (Mo–O distance changes from 2.21 to 3.81 Å), producing an intermediate stage where the CO_2 still remains attached to the active site through the S_i–C bond. After the break of the Mo–O bond, the Mo–S_i bond length decreases from 2.54 to 2.34 Å. The charge distribution is conserved during the reaction, being mainly localized on the dimethyl dithiolene ligands (−1.33 a.u.) and around the –CO_2 group (−0.75 a.u.). This reaction needs E_a = 13.3 kcal/mol, is

Scheme 4 Formate oxidation and C–H bond cleavage (the total charge and multiplicity of the system are in *brackets*)

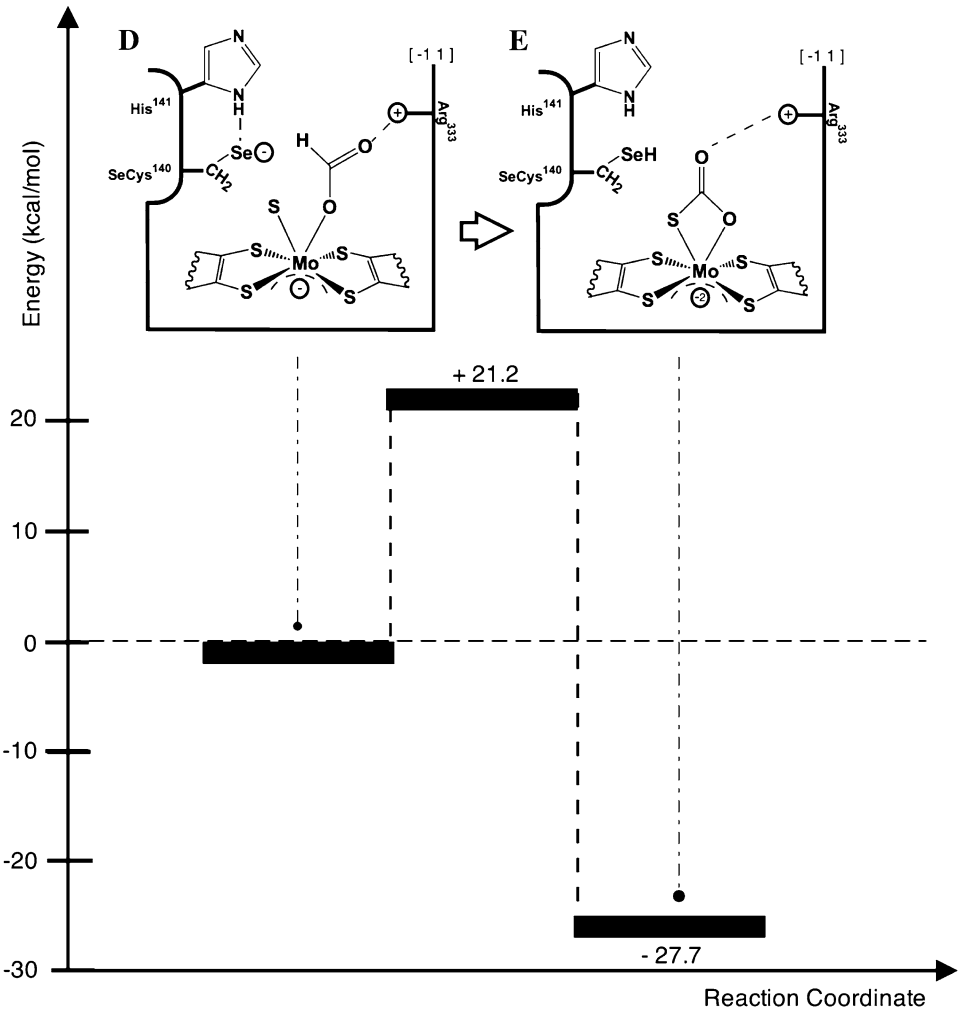

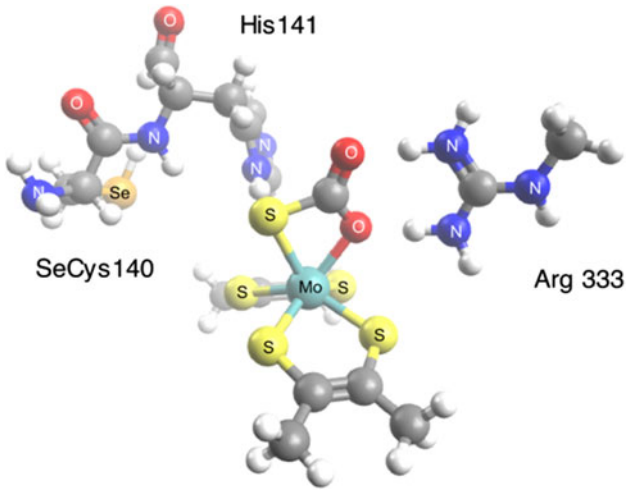

Fig. 4 Product obtained after the proton transfer reaction from formate to SeCys[140]

endothermic ($E_r = 7.2$ kcal/mol), and yielded a transition state characterized by one imaginary frequency of 67i cm^{-1}.

To complete the product release, the S_i–C bond must be broken. This happens when the S_i–$C_{formate}$ distance increases from 1.89 Å in the reactants to 2.20 Å in the transition state (123i cm^{-1}). In the product, the CO_2 molecule is found at 3.81 Å (S_i–C distance) as a neutral molecule (charge −0.05 a.u.). This reaction yielded $E_a = 4.5$ kcal/mol and $E_r = -7.8$ kcal/mol, indicating the two-step process of CO_2 release is almost thermoneutral (−0.6 kcal/mol).

In the second case (not shown), it was assumed that after the transfer of the proton of the formate to the SeCys residue, two electrons would be immediately transferred to the redox centers included in the electron transfer pathway of the protein [9, 10]. This implies the two-electron oxidation of the active site, for which it was necessary to manually adjust the charge of the model to +1. Compared with the model previous to these modifications, the only changes are the Mo–S_i and Mo–$O_{formate}$ bond lengths, decreasing from 2.54 to 2.39 Å and from 2.21 to 2.15 Å, respectively. The negative charge remains located in the –CO_2 group, whereas the dithiolene ligands become

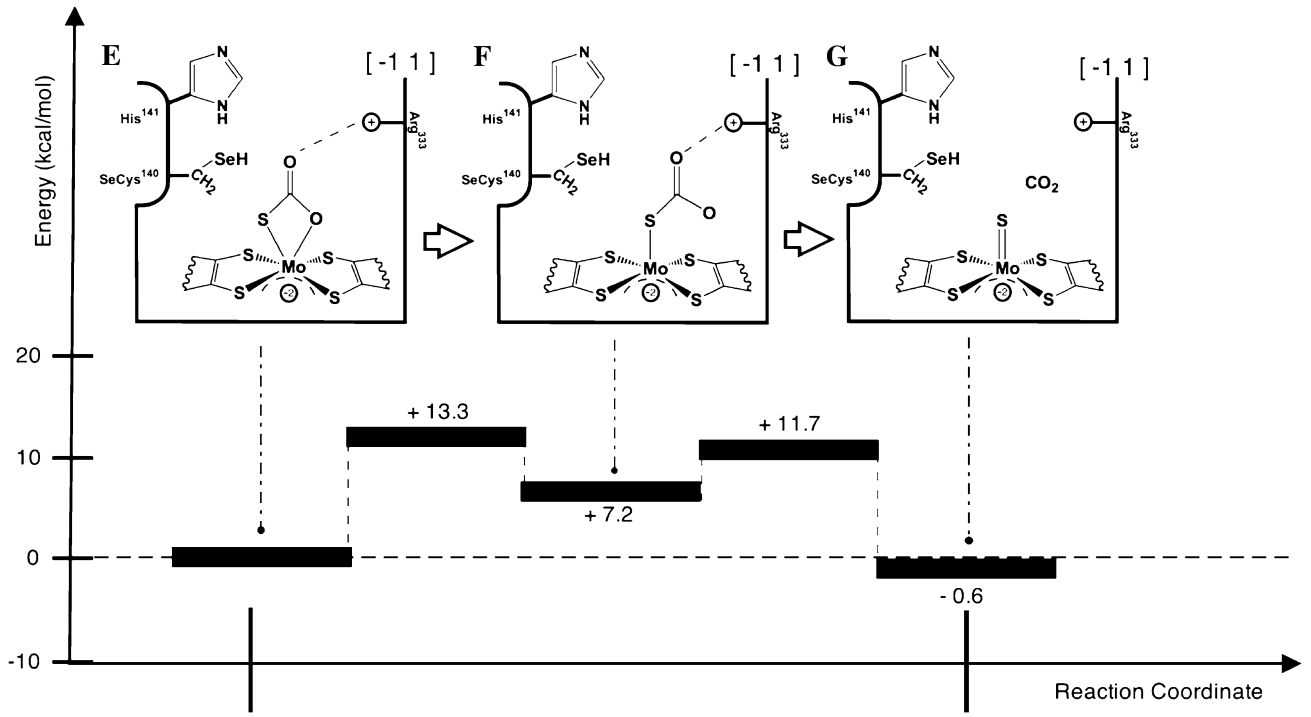

Scheme 5 Carbon dioxide release mechanism preceding the oxidation of the active site (the total charge and multiplicity of the system are in *brackets*)

positively charged. In the transition state (imaginary frequency of 127.91i cm^{-1}) it can be noted that both the Mo–O and the S_i–C bonds are simultaneously broken at the same time as the Mo–S_i bond length is stretched to 2.12 Å. In the products of this reaction, the dissociation of the CO_2 molecule is accomplished and similarly to what happens in the first hypothesis, the S_i becomes double-bonded to the molybdenum. This reaction requires an activation energy of 25.6 kcal/mol and is exothermic by −16.6 kcal/mol.

Analyzing the activation energy profiles for the two hypotheses tested for CO_2 release, we found that the first hypothesis emerges as more probable, even though it needs two steps to release the product.

Regeneration of the active site to the initial state

On the basis of the complex obtained after CO_2 release, the last steps of the proposed catalytic mechanism will involve the transfer of the proton attached to the SeCys residue, oxidation of the active site from Mo(IV) to Mo(VI), and binding of the SeCys residue to the molybdenum ion. The proton transfer process could be assisted by solvent molecules or by some neighboring amino acid residues. However, because there are no experimental data about how this is accomplished, the only thing that we were able to model was the binding of the resulting anionic SeCys residue to the Mo(VI) ion in the oxidized active site. In this sense, it is expected that the loop in which the SeCys residue is located undergoes a conformational rearrangement.

To model this reaction, the proton of the SeCys residue was manually deleted and the charge of the system was adjusted to obtain a molybdenum ion in the +6 formal oxidation state to emulate the reoxidation of the active site. As expected, the overall charge of the active site became more positive. The charge of the S_i ligand changed from −0.63 to 0.19 a.u. without Mo–S_i bond length modification (from 2.15 to 2.14 Å). The anionic selenium, with a charge of −0.71 a.u., is 3.52 Å from the S_i ligand and interacts very closely with His^{141} (2.64 Å) through a hydrogen bond with the imidazole NH group. From this point, two pathways that will depend on the presence or absence of a substrate molecule near the active site can be drawn. For the first pathway, the active site structure in the absence of formate returns to the initial state, in which both the selenium atom and the S_i ligand are bound to the Mo(VI) ion. The computational results indicate that this process requires two steps and is energetically feasible (Scheme 6). The first step implies the binding of the selenium atom to the S_i ligand. This process yielded $E_a = 2$ kcal/mol and is exothermic by −18 kcal/mol. The optimized geometry of the transition state (imaginary frequency of 33i cm^{-1}) reveals that the selenium atom is 2.25 Å from the S_i ligand and 3.35 Å from the molybdenum ion. In the product of this reaction, the Mo–S_i bond length increases from 2.14 to 2.35 Å, indicating that the Mo–S_i double bond become a single bond upon

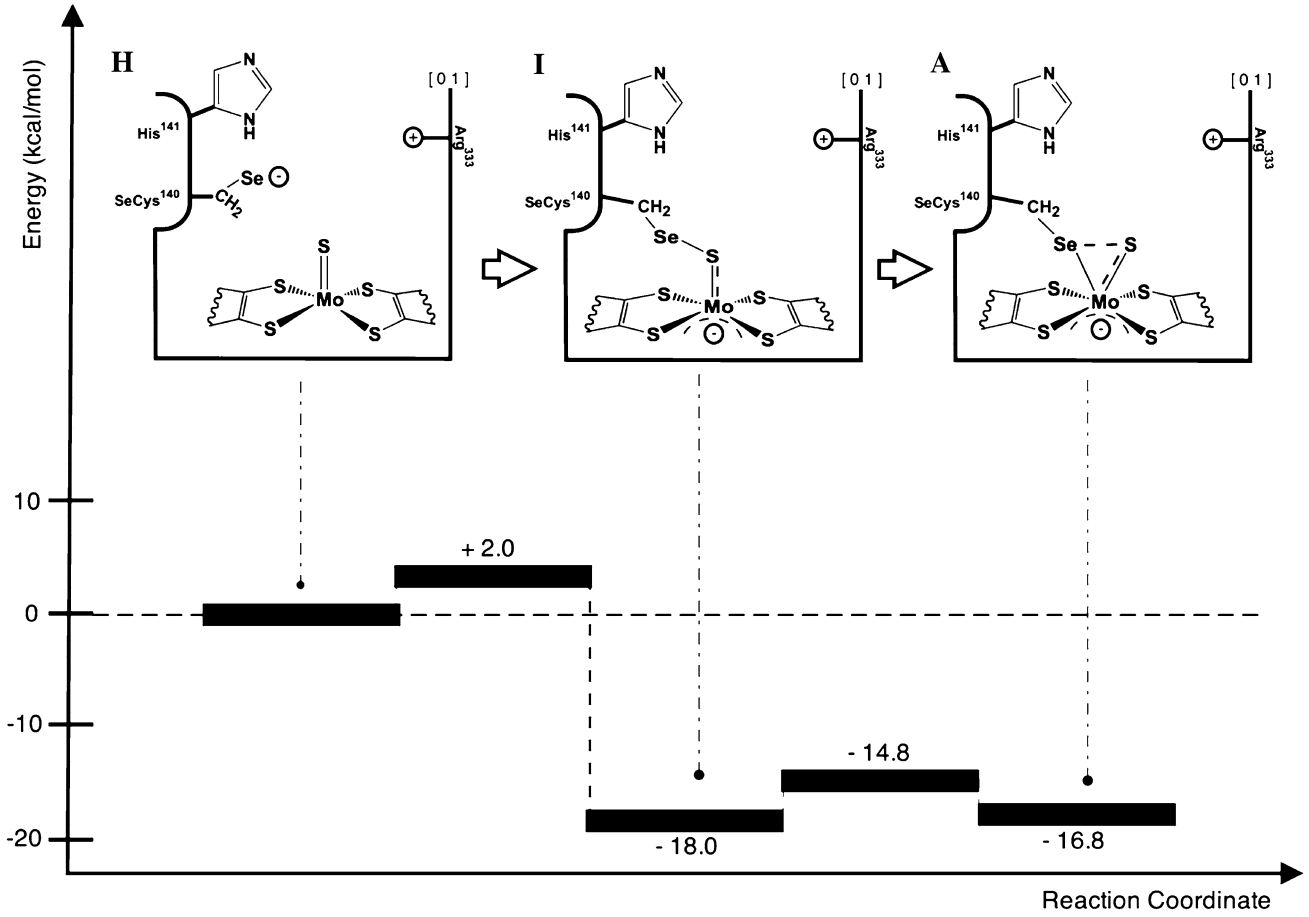

Scheme 6 Regeneration of the active site to the initial oxidized state (the total charge and multiplicity of the system are in *brackets*)

selenium atom binding. In spite of this rearrangement, the selenium atom does not bind the molybdenum ion, remaining 3.94 Å away. The charge distribution remains almost unaltered (−0.67 a.u. in each dithiolene ligand, −0.34 a.u. in the S_i, and −0.24 a.u. in the selenium). After Se–S_i bond formation, the SeCys residue binds the Mo(VI) ion and the S_i as in the initial state. The calculations yielded $E_a = 3.2$ kcal/mol and $E_r = 1.2$ kcal/mol. The optimized geometry of the transition state (imaginary frequency of 37.68i cm^{-1}) shows that the selenium atom approaches the molybdenum ion (from 3.94 to 3.35 Å) and that the charge distribution and the Mo–S_i and Se–S_i bond lengths remain unaltered. In the product, the SeCys residue binds the molybdenum ion and the S_i ligand through single bonds (2.96 and 2.26 Å, respectively).

The second pathway is summarized in Scheme 7. The computational results showed that binding of a new formate molecule to the oxidized active site (as found in the starting species in Scheme 6) is a one-step process requiring only $E_a = 6.1$ kcal/mol and $E_r = 2.7$ kcal/mol (Scheme 7). In the transition state (imaginary frequency of 45i cm^{-1}) the Mo–S_i bond length is unaltered but the S_i ligand is pushed aside, creating space for the incoming formate molecule (Mo–$O_{formate}$ bond length 3.03 Å). In the product of the reaction the formate binds the molybdenum ion (Mo–$O_{formate}$ bond length 2.21 Å) and the S_i ligand gains negative charge (−0.62 a.u.). Similar to what was observed before, the conserved Arg^{333} has a key role in this reaction driving and stabilizing the formate anion by hydrogen bonds. However, there is a striking difference when the formate anion binds the active site in the situation presented in Scheme 7 (SeCys residue not bound to the S_i ligand), as the energy cost of binding a new substrate molecule is 14 kcal/mol less than that obtained with the SeCys bound to the S_i ligand (Scheme 2). This difference, which is attributed to the different charge distribution and steric hindrance of the complex when the SeCys residue binds the S_i ligand, indicates that the catalytic cycle should follow this pathway instead of regenerating the active site as in the initial state.

Discussion

Scheme 8 summarizes the main conclusions on the general catalytic mechanism of metal-dependent Fdh evaluated through DFT tools. The first part of this study demonstrated

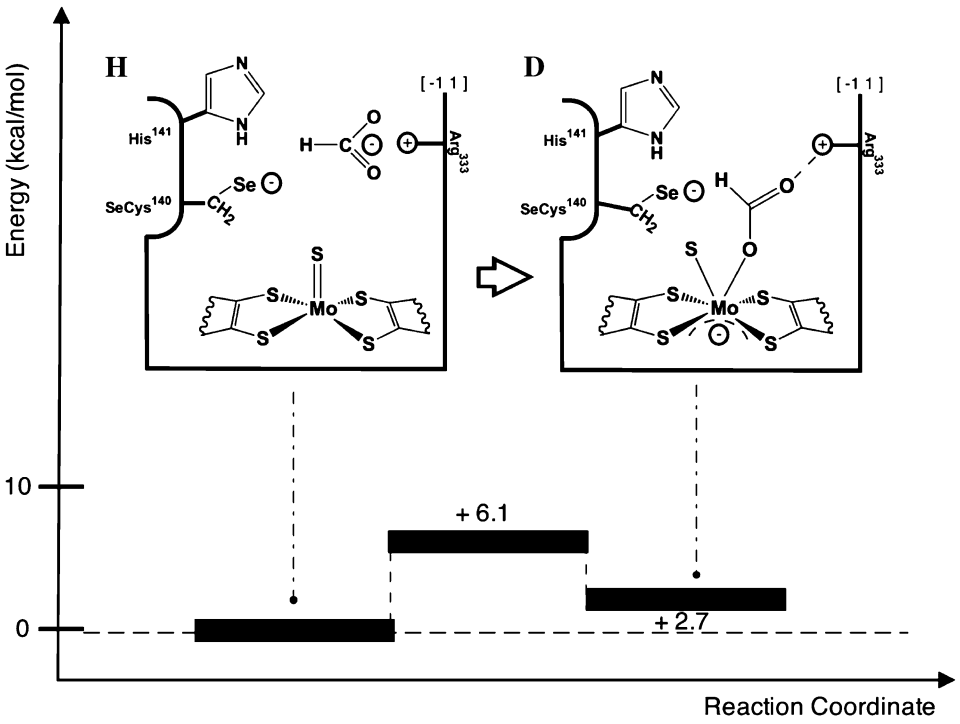

Scheme 7 Formate binding to an intermediate species produced after oxidation of the active site (the total charge and multiplicity of the system are in *brackets*)

that the hexacoordinated molybdenum ion of the crystallographic structure is in the +6 oxidation state (Fig. 3a, Scheme 8, state A). Previous studies of *D. desulfuricans* Fdh demonstrated that this state represents an inactive form of the enzyme resulting from the aerobic purification procedure of an enzyme that works physiologically under strict anaerobic conditions [15]. This is corroborated with all the Fdh enzymes studied in this work, as they needed to be incubated with the substrate prior to electron acceptor addition to obtain their maximal specific activity (Fig. S1). This activation step implies that the enzyme performs at least one complete turnover returning to a Mo(VI) state (Scheme 8, state H) different from the initial one (Scheme 8, state A). Then, the reaction proceeds with the formate molecule binding the active site in a state where the Mo(VI) ion has an available binding position (Scheme 8, step H–D). This is indicated by the results summarized in Scheme 7, where the binding of the formate to the pentacoordinated Mo(VI) ion has $E_a = 6.1$ kcal/mol. In summary, the three initial steps with high activation energies (Scheme 8, steps A–B, B–C, and C–D, $E_a = 15.5$, 20.0, and 18.4 kcal/mol, respectively) represent the activation route necessary to perform the first cycle of the catalytic mechanism starting from the aerobically inactive enzyme. Step B–C in Scheme 8, which involves the process identified as a sulfur shift, is similar to that proposed for the catalytic mechanism of periplasmic nitrate reductase where the role of the SeCys residue is performed by a cysteine residue [37, 38]. This may indicate that the sulfur shift could be a common mechanism by which these enzymes enable a free coordinating position on the metal ion for substrate coordination.

The formate oxidation process also involves the participation of amino acids that are conserved in all metal-dependent Fdhs characterized so far. Our DFT calculations indicate that the side chain of the arginine residue interacts with both the substrate and the product of the reaction, guiding the substrate to the active site, stabilizing it, and driving the product release. In this sense, the positively charged side chain of arginine cancels the negative charge of the formate anion, facilitating its interaction with the active site.

One of the most intriguing roles to unveil was that of the conserved histidine residue. Khangulov et al. [5] have proposed that this residue might be involved in the deprotonation of the SeCys following the proton transfer reaction from the substrate to the selenide anion. In contrast, our calculations indicate that an NH group of the imidazole ring of histidine stabilizes the selenide anion through hydrogen bonds (Scheme 3). This role is also supported by the fact that, when the conserved histidine is not included in the model, the formation of the selenide anion yields an unstable transition state which results in a very high activation energy (E_a ~45 kcal/mol). These results also suggest why metal-dependent Fdhs contain a SeCys residue instead of a regular cysteine residue, as found in periplasmic nitrate reductases. The SeCys and cysteine side chains have pK_a values of 5.2 and 8.2, respectively. This indicates that under physiological conditions (pH ~7.00) the selenium atom of the SeCys residue

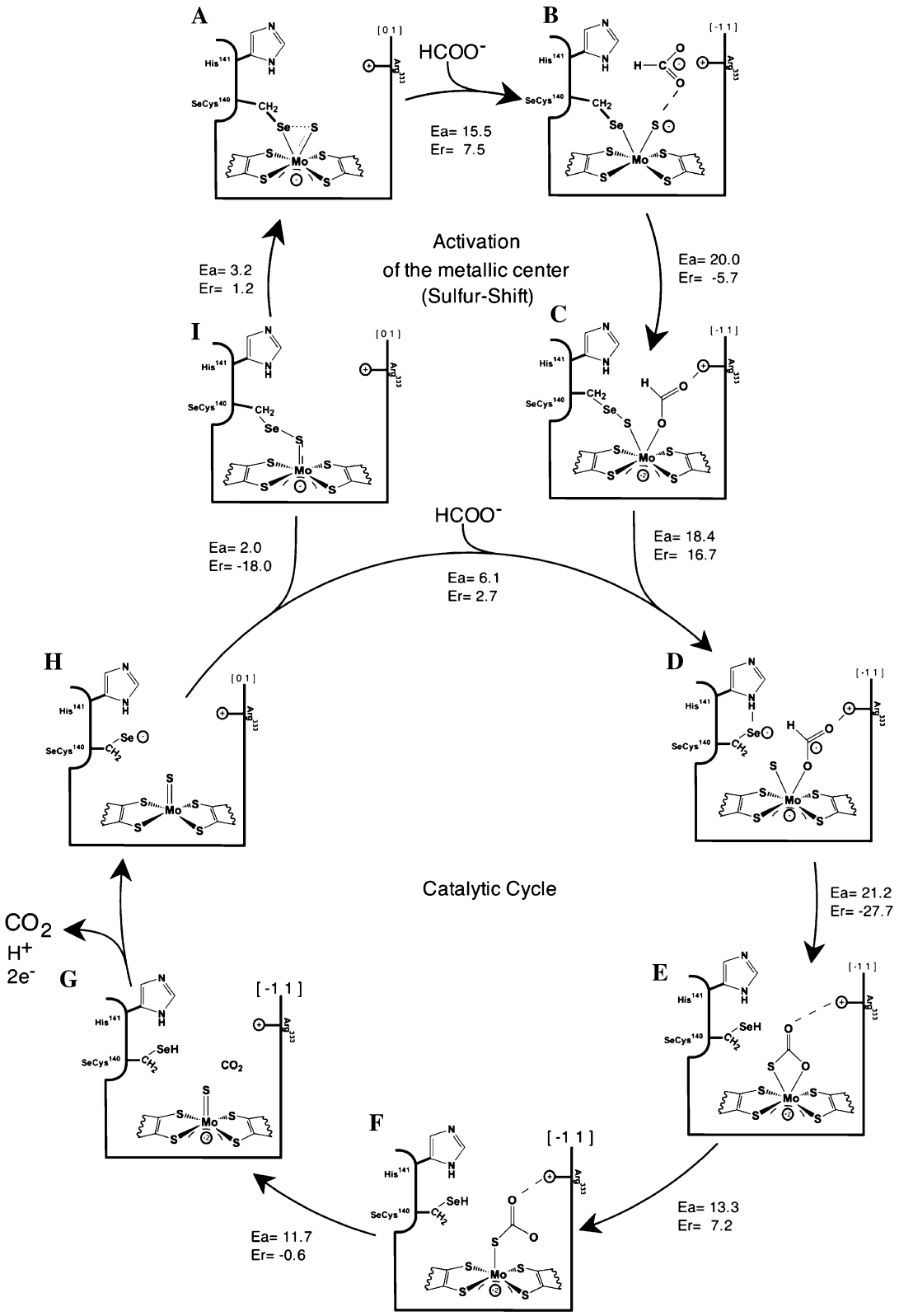

Scheme 8 Global view of the catalytic mechanism of metal-dependent formate dehydrogenase (E_a and E_r in kilocalories per mole)

can be found in the anionic form after breaking of the bond with the S_i ligand bound to the molybdenum ion. Owing to the high pK_a of the side chain of a cysteine residue, the presence of a stable cysteinate at physiological pH is unlikely. This statement has strong experimental support from early studies performed in *E. coli* Fdh-H, in which it was demonstrated that mutating the SeCys to a cysteine almost inactivates the enzyme, lowering the k_{cat} by more than 2 orders of magnitude (from 2,800 to 9 s^{-1}) [39].

The kinetic studies of the enzyme with the isotopically enriched ^{2}HCOONa clearly indicate that the C–H bond break is involved in the rate-limiting step of the catalytic mechanism. Analyzing the activation energy values for every step of the simulated mechanism, and having in mind that the three initial steps of the mechanism (Scheme 8, steps A–B, B–C, and C–D) do not take part in the enzymatic catalytic cycle, we can note that the highest activation energy barrier involves the transfer of the proton from the substrate to the selenium (21.2 kcal/mol, Scheme 8, step D–E), suggesting that, in agreement with the experimental results, this is the rate-limiting event of the catalytic mechanism.

Comparing metal-dependent Fdhs and eukaryotic NAD^+-dependent Fdhs, a key difference is evident in the enzymatic mechanism of formate oxidation to carbon dioxide. Metal-dependent Fdhs catalyze the transfer of a proton from the substrate to the enzyme, whereas, according to the currently accepted mechanism, NAD^+-dependent Fdhs catalyze the transfer of a hydride to the NAD^+ cofactor to produce an NADH [40]. Our results indicate that this fundamental difference results from the nature of the group that accepts the hydrogen ion from the substrate, i.e., a nucleophilic selenide anion versus a NAD^+ cation.

Acknowledgments C.S.M. thanks Fundação para a Ciência e a Tecnologia for funding (grant SFRH/BD/32478/2006). P.J.G. and N.M.F.S.A.C. thank Programa Ciência 2007 and 2008 of Fundação para a Ciência e a Tecnologia. This work was supported by projects PDCT/QUI/57701/2004 and PTDC/QUI/67052/2006 in Portugal and CAID-UNL, CONICET, and SEPCYT in Argentina. C.D.B. thanks to CONICET (Argentina).

References

1. Alberty RA (2001) Arch Biochem Biophys 389:94–109
2. Heidelberg JF, Seshadri R, Haveman SA, Hemme CL, Paulsen IT, Kolonay JF, Eisen JA, Ward N, Methe B, Brinkac LM, Daugherty SC, Deboy RT, Dodson RJ, Durkin AS, Madupu R, Nelson WC, Sullivan SA, Fouts D, Haft DH, Selengut J, Peterson JD, Davidsen TM, Zafar N, Zhou L, Radune D, Dimitrov G, Hance M, Tran K, Khouri H, Gill J, Utterback TR, Feldblyum TV, Wall JD, Voordouw G, Fraser CM (2004) Nat Biotechnol 22:554–559
3. Richardson DJ (2000) Microbiology 146(3):551–571
4. Boyington JC, Gladyshev VN, Khangulov SV, Stadtman TC, Sun PD (1997) Science 275:1305–1308
5. Khangulov SV, Gladyshev VN, Dismukes GC, Stadtman TC (1998) Biochemistry 37:3518–3528
6. Jormakka M, Tornroth S, Byrne B, Iwata S (2002) Science 295:1863–1868
7. Jormakka M, Tornroth S, Abramson J, Byrne B, Iwata S (2002) Acta Crystallogr D Biol Crystallogr 58:160–162
8. Gladyshev VN, Boyington JC, Khangulov SV, Grahame DA, Stadtman TC, Sun PD (1996) J Biol Chem 271:8095–8100
9. Moura JJ, Brondino CD, Trincao J, Romao MJ (2004) J Biol Inorg Chem 9:791–799
10. Brondino CD, Rivas MG, Romao MJ, Moura JJ, Moura I (2006) Acc Chem Res 39:788–796
11. Raaijmakers H, Teixeira S, Dias JM, Almendra MJ, Brondino CD, Moura I, Moura JJ, Romao MJ (2001) J Biol Inorg Chem 6:398–404
12. Raaijmakers H, Macieira S, Dias JM, Teixeira S, Bursakov S, Huber R, Moura JJ, Moura I, Romao MJ (2002) Structure 10:1261–1272
13. Raaijmakers HC, Romao MJ (2006) J Biol Inorg Chem 11:849–854
14. Costa C, Teixeira M, LeGall J, Moura JJG, Moura I (1997) J Biol Chem 2:198–208
15. Rivas MG, Gonzalez PJ, Brondino CD, Moura JJ, Moura I (2007) J Inorg Biochem 101:1617–1622
16. Leopoldini M, Chiodo SG, Toscano M, Russo N (2008) Chemistry 14:8674–8681
17. Liu MC, Peck HD Jr (1981) J Biol Chem 256:13159–13164
18. Legall J, Mazza G, Dragoni N (1965) Biochim Biophys Acta 99:385–387
19. Mota CS, Valette O, Gonzalez PJ, Brondino CD, Moura JJG, Moura I, Dolla A, Rivas MG (2010) J Bacteriol 193:2917–2923
20. Almendra MJ, Brondino CD, Gavel O, Pereira AS, Tavares P, Bursakov S, Duarte R, Caldeira J, Moura JJ, Moura I (1999) Biochemistry 38:16366–16372
21. Roux B (1995) Comput Phys Commun 91:275–282
22. Ensing B, De Vivo M, Liu Z, Moore P, Klein ML (2006) Acc Chem Res 39:73–81
23. Huber T, Torda AE, van Gunsteren WF (1994) J Comput Aided Mol Des 8:695–708
24. Laio A, Parrinello M (2002) Proc Natl Acad Sci USA 99:12562–12566
25. Berg BA, Neuhaus T (1991) Phys Lett B 267:249–253
26. Ramos MJ, Fernandes PA (2008) Acc Chem Res 41:689–698
27. Castillo R, Oliva M, Marti S, Moliner V (2008) J Phys Chem B 112:10012–10022
28. Becke AD (1993) J Chem Phys 98:5648–5652
29. Lee CT, Yang WT, Parr RG (1988) Phys Rev B 37:785–789
30. Stephens PJ, Devlin FJ, Chabalowski CF, Frisch MJ (1994) J Phys Chem 98:11623–11627
31. Vosko SH, Wilk L, Nusair M (1980) Can J Phys 58:1200–1211
32. Cerqueira NM, Fernandes PA, Eriksson LA, Ramos MJ (2006) Biophys J 90:2109–2119
33. Cerqueira NMFSA, Fernandes PA, Eriksson LA, Ramos MJ (2004) J Mol Struct Theochem 709:53–65
34. Himo F (2006) Theor Chem Acc 116:232–240
35. Cerqueira NMFSA, Fernandes PA, Ramos MJ (2011) J Chem Theory Comput 7:1356–1368
36. Axley MJ, Grahame DA (1991) J Biol Chem 266:13731–13736
37. Cerqueira NM, Gonzalez PJ, Brondino CD, Romao MJ, Romao CC, Moura I, Moura JJ (2009) J Comput Chem 30:2466–2484
38. Najmudin S, Gonzalez PJ, Trincao J, Coelho C, Mukhopadhyay A, Cerqueira NM, Romao CC, Moura I, Moura JJ, Brondino CD, Romao MJ (2008) J Biol Inorg Chem 13:737–753
39. Axley MJ, Bock A, Stadtman TC (1991) Proc Natl Acad Sci USA 88:8450–8454
40. Castillo R, Oliva M, Marti S, Moliner V (2008) J Phys Chem B 112:10012–10022